2014 IEEE International Conference on Robotics & Automation (ICRA)
Hong Kong Convention and Exhibition Center
May 31 - June 7, 2014. Hong Kong, China

Tether-guided landing of unmanned helicopters without GPS sensors*

L.A. Sandino[1], D. Santamaria[2], M. Bejar[3], A. Viguria[2], K. Kondak[4] and A. Ollero[1,2]

***Abstract*— Landing of unmanned helicopters is a challenging maneuver which can be seriously affected by GPS sensor reliability. This work explores an alternative approach to GPS sensors to avoid typical drawbacks, such as inaccuracies of standalone sensors or weight/cost for Real Time Kinematic (RTK) setups. To this end, the paper studies a setup consisting of a tether linking the helicopter to the landing point. Appropriate sensing of tether attitude relative to the helicopter together with an altitude measurement, allows estimation of the helicopter's linear position relative to the landing point. Additionally, the tension exerted on the tether provides a stabilizing effect on helicopter translational dynamics. Taking into account all these considerations, a model-based control strategy is developed and implemented in the real platform. The experimental results endorse the validity of the proposed approach.**

***Keywords*—Unmanned aerial systems, tethered helicopter, modeling, model-based control, position estimate, landing**

I. Introduction

When comparing different Unmanned Aerial Vehicle (UAV) configurations, helicopters and other rotor-based aircraft have capabilities such as hovering and vertical take-off and landing that cannot be achieved by conventional fixed-wing aircraft. These features allow remotely piloted and autonomous helicopters to be used extensively nowadays for applications such as inspection, accurate measurement and other aerial robotic applications. However, hovering and landing performance can be seriously affected by wind disturbances or sensor failures.

This paper presents a tethered setup that improves system operation under such difficulties. This augmented setup consists of a tether linking the helicopter to the landing point. The application of tension on the tether at all times is a crucial feature for system operation. In order to address the sensor reliability issue, the often problematic GPS measurement is replaced in this work by an alternative linear position estimation relative to tether's fixed point at ground, based on helicopter altitude and tether attitude relative to the airframe. This sensing approach makes the system more robust since it will work even when GPS is jammed, and provides sufficient information for a tether-guided landing. An additional benefit of tether use is that tension exerted provides robustness against external disturbances.

To the best of the authors' knowledge, the tether-based estimate for replacing GPS sensors in landing is really a new line of research since no references can be found in the existing literature. In the application scenario of landing a helicopter using a tether as an additional control resource, the only contributions are those of [1], [2]. Concerning performance degradation under wind disturbance, the use of tether tension to increase hovering maneuver stability was also almost unexplored before the authors' first contributions [3], [4]. The only related precedents that consider a tethered configuration for rotorcraft prototypes are those of [5], where the linearized equations describing the perturbed longitudinal motion of a tethered rotorcraft are presented and [6], where a discussion of control and stability problems involved in the tethered configuration for a rotor platform prototype is presented, with special emphasis on tether dynamics.

This paper is organized as follows. Section II presents the dynamic model corresponding to the augmented system (small-size helicopter and tether) as well as subsequent analysis to underline the benefits of the tethered configuration in stabilizing translational dynamics. The helicopter control approach together with the novel methodology based on the tethered setup for estimating linear position relative to the landing point, are presented in Section III. In Section IV, the experimental setup is described in detail, and the data gathered in the field is discussed. Finally, Section V is devoted to conclusions and future work.

II. System modeling and analysis

This section presents the resulting model for the tethered configuration (see Fig. 1). A more detailed derivation following Kane's methodology [7] can be found in previous works of the authors [8]. The section ends with an analysis of the potentials of the tethered setup.

A. Helicopter model

Dynamics of a small-size helicopter with a stiff main rotor are mainly described by a mechanical model. Attempts to include an elaborate aerodynamic model of the main rotor in controller design do not show significant improvements in performance during control experiments. This could be considered evidence for the fact that the approach to analyzing helicopter behavior by means of a mechanical model is suitable for practical applications [9].

The mechanical characterization of the helicopter accounts for two separate rigid bodies, fuselage F (with mass m_F)

*This work is supported by Excellence Project of Junta de Andalucía RURBAN (P09-TIC-5121), Spanish Government RD&I National Plan Project CLEAR (DPI2011-28937-C02-01) and European Commission Project EC-SAFEMOBIL (FP7-ICT-2011-7)

[1]L.A. Sandino and A. Ollero are with GRVC, University of Seville, Seville, SPAIN (✉) lsandino at us.es

[2]D. Santamaria, A. Viguria and A. Ollero are with Center for Advanced Aerospace Technologies (CATEC), Seville, SPAIN dsantamaria, aviguria, aollero at catec.aero

[3]M. Bejar is with GRVC, University Pablo de Olavide, Seville, SPAIN mbejdom at upo.es

[4]K. Kondak is with German Aerospace Agency (DLR), Oberpfaffenhofen, GERMANY konstantin.kondak at dlr.de

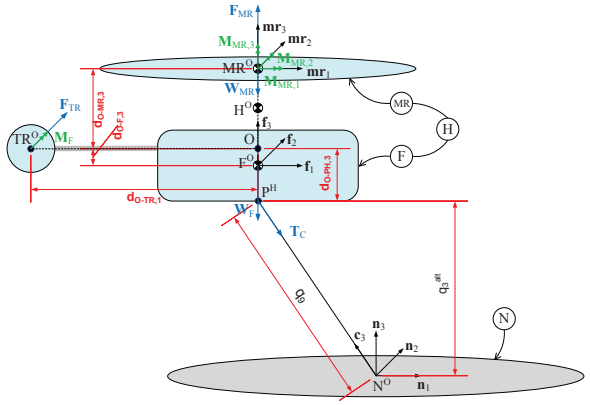

Fig. 1: Tethered helicopter scheme: description of reference frames (N, F, MR) , centers of mass (F^O, MR^O, H^O), points (TR^O, O, P^H), dimensions ($d_{O-P,i}$) of interest, forces and moments applied to the helicopter

and stiff main rotor MR (modeled as a thin solid disk with mass m_{MR} and constant angular speed ω_{MR}), whereas the tail rotor TR^O will only act as a force application point on the fuselage. This characterization arises from the fact that for most commercially available small-size helicopters, the inertial effects of the main rotor (gyroscopic effect) become the main component influencing the rotational dynamics of the whole mechanical system, whilst the tail rotor inertial influence is negligible.

Concerning forces and moments applied to the helicopter, the main rotor generates a force $\mathbf{F}_{MR} = f_{MR,3}\mathbf{f_3}$ applied at center of mass MR^O, and moments $\mathbf{M}_{MR,i} = t_{MR,i}\mathbf{f_i}\,(i = 1,2,3)$ applied to rigid body MR, whereas the tail rotor generates a force $\mathbf{F}_{TR} = f_{TR,2}\mathbf{f_2}$ applied at point TR^O, and a moment $\mathbf{M}_F = t_{TR,2}\mathbf{f_2}$ applied to rigid body F. The force of gravity $\mathbf{W}_j = -m_j g\mathbf{n_3}\,(j = F, MR)$ applied at centers of mass F^O and MR^O is also considered, where g is the acceleration of gravity.

Kinematic differential equations for translation are:

$$\dot{q}_i = u_i \quad (i = 1,2,3) \tag{1}$$

whereas those for rotation are:

$$\begin{aligned}
\dot{q}_4 &= -\left(s_6u_5 - c_6u_4\right)/c_5 \\
\dot{q}_5 &= s_6u_4 + c_6u_5 \\
\dot{q}_6 &= u_6 + s_5\left(s_6u_5 - c_6u_4\right)/c_5
\end{aligned} \tag{2}$$

where $q_i(t)\,(i = 1,2,3)$ and $u_i(t)\,(i = 1,2,3)$ are, respectively, the generalized coordinates and generalized speeds describing the position $\mathbf{p}^{N^O \to H^O}$ and velocity ${}^N\mathbf{v}^{H^O}$ of center of mass H^O in inertial reference frame N; $q_i(t)\,(i = 4,5,6)$ are the Euler angles in body1-2-3 order (roll, pitch and yaw) describing the orientation of frame F in inertial reference frame N; $u_i(t)\,(i = 4,5,6)$ are generalized speeds describing angular velocity ${}^N\boldsymbol{\omega}^F$ expressed in axes of frame F; and $s_i = \sin(q_i)$, $c_i = \cos(q_i)$.

The resulting dynamic differential equations for translation following Kane's methodology [7] are:

$$\begin{aligned}
m_H\dot{u}_1 &= f_{MR,3}s_5 - f_{TR,2}c_5s_6 \\
m_H\dot{u}_2 &= f_{TR,2}\left(c_4c_6 - s_4s_5s_6\right) - f_{MR,3}s_4c_5 \\
m_H\dot{u}_3 &= f_{MR,3}c_4c_5 + f_{TR,2}\left(s_4c_6 + c_4s_5s_6\right) - m_Hg
\end{aligned} \tag{3}$$

while for rotation they are:

$$\begin{aligned}
I_{H11}\dot{u}_4 &= t_{MR,1} + d_{O-H^O,3}f_{TR,2} + \\
&\quad + \left(\left(I_{H22} - I_{H33}\right)u_6 - 2I_{MR11}\omega_{MR}\right)u_5 \\
I_{H22}\dot{u}_5 &= t_{MR,2} + t_{TR,2} + \\
&\quad + \left(\left(I_{H33} - I_{H11}\right)u_6 + 2I_{MR11}\omega_{MR}\right)u_4 \\
I_{H33}\dot{u}_6 &= t_{MR,3} + d_{O-TR^O,1}f_{TR,2} + \\
&\quad + \left(I_{H11} - I_{H22}\right)u_4u_5
\end{aligned} \tag{4}$$

where $m_H = m_F + m_{MR}$ is the total mass, I_{MR11} is the principal moment of inertia of rigid body MR, $I_{Hii}\,(i = 1,2,3)$ are the principal moments of inertia corresponding to the whole system, and $d_{O-H^O,3} = \left(m_F \cdot d_{O-F^O,3} + m_{MR} \cdot d_{O-MR^O,3}\right)/m_H$.

Since only the mechanical model is used for modeling analysis and subsequent derivation of the controller, as aforesaid, the forces and moments exerted on the system will be considered as system inputs for control design. More precisely, the subset of these forces and moments whose values can be fixed independently of each other by the controller, is given by $f_{MR,3}$, $t_{MR,1}$, $t_{MR,2}$ and $f_{TR,2}$. In the implementation of the controller, these inputs are transformed to servo positions using simple linear functions with only three unknown constants: the first constant describes the relation between the main rotor collective pitch and lifting force $f_{MR,3}$; the second, the relation between the main rotor cyclic pitches and moments $t_{MR,1}$ and $t_{MR,2}$, and the third the relation between the tail rotor collective pitch and force $f_{TR,2}$. These constants are identified experimentally. This approach to linear characterization of aerodynamics has already been verified successfully in [9].

B. Tethered helicopter model

When accounting for the tether effect on the model, it is assumed for the sake of simplicity that the tether end at the ground coincides with the origin of inertial frame N. At the other end, the tether is connected to the helicopter at point P^H as depicted in Fig. 1. For this configuration,the resulting dynamic model is more manageable when helicopter position in inertial frame N is defined by means of the generalized coordinates $q_{7,8,9}(t)$. As can be seen in Fig. 2, the device fixing the tether to the helicopter is a universal joint, denoted by frame C. Therefore, angular variables $q_{7,8}(t)$ correspond to two successive rotations at point P^H that align vector $\mathbf{f_3}$ of the fuselage frame with the tether line defined by vector $\mathbf{c_3}$. The remaining configuration coordinate $q_9(t)$ defines the instantaneous tether length, as shown in Fig. 1. Hence, the position of point P^H is given by:

$$\mathbf{p}^{N^O \to P^H} = q_9\mathbf{c_3} \tag{5}$$

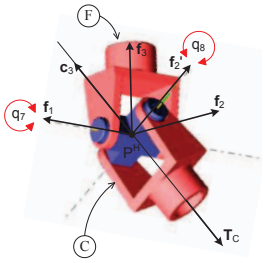

Fig. 2: Universal joint scheme at point P^H

TABLE I: Direction cosine matrices ${}^N DCM^F$ and ${}^F DCM^C$

	$\mathbf{f}_1$	$\mathbf{f}_2$	$\mathbf{f}_3$
$\mathbf{n}_1$	$c_5 c_6$	$-c_5 s_6$	s_5
$\mathbf{n}_2$	$c_4 s_6 + s_4 s_5 c_6$	$c_4 c_6 - s_4 s_5 s_6$	$-s_4 c_5$
$\mathbf{n}_3$	$s_4 s_6 - c_4 s_5 c_6$	$s_4 c_6 + c_4 s_5 s_6$	$c_4 c_5$

	$\mathbf{c}_1$	$\mathbf{c}_2$	$\mathbf{c}_3$
$\mathbf{f}_1$	c_8	0	s_8
$\mathbf{f}_2$	$s_7 s_8$	c_7	$-s_7 c_8$
$\mathbf{f}_3$	$-c_7 s_8$	s_7	$c_7 c_8$

where $s_i = \sin(q_i)$ and $c_i = \cos(q_i)$

whereas the tether tension vector is defined by:

$$\mathbf{T}_C = -T_C \mathbf{c_3} \tag{6}$$

The use of angular variables $q_{7,8}$ and tether length q_9 as configuration variables for helicopter position while motion variables $u_{1,2,3}$ remain Cartesian, requires a new analysis of the system kinematics. To this end, the expression

$$\begin{aligned} \mathbf{p}^{N^O \to H^O} &= \mathbf{p}^{N^O \to P^H} + \mathbf{p}^{P^H \to O} + \mathbf{p}^{O \to H^O} \\ \sum_{i=1}^{3} (q_i \mathbf{n_i}) &= q_9 \mathbf{c_3} + d_{P^H - H^O,3} \mathbf{f_3} \end{aligned} \tag{7}$$

where $d_{P^H - H^O,3} = d_{O-H^O,3} - d_{O-P^H,3}$, is derived with respect to time and then solved for $\dot{q}_{7,8,9}$, which yields:

$$\begin{bmatrix} \dot{q}_7 & \dot{q}_8 & \dot{q}_9 \end{bmatrix}^T = \mathbf{M}^{3\times 6}(q_{4,\cdots,9}) \cdot \begin{bmatrix} u_1 & \cdots & u_6 \end{bmatrix}^T \tag{8}$$

While it is true that kinematic equations (8) are more complex than those of (1) ($\mathbf{M}$ is a dense matrix), the real advantage of using these new configuration variables $q_{7,8,9}$ while maintaining Cartesian motion variables $u_{1,2,3}$ is given by the resulting dynamic differential equations, much more compact for the tethered configuration than those corresponding to Cartesian coordinates for both configuration ($q_{1,2,3}$) and motion variables. Derivation of (7) is made taking into account that dextral sets of orthogonal unit vectors $\mathbf{c_i}$, $\mathbf{f_i}$ and $\mathbf{n_i}$ $(i = 1, 2, 3)$ fixed respectively in frames C, F and N, are geometrically related by the direction cosine matrices shown in Table I.

Finally, the resulting dynamic differential equations for translation in the tethered configuration are:

$$\begin{aligned} m_H \dot{u}_1 &= RHS_1 - T_C \cdot {}^N DCM^C[1,3] \\ m_H \dot{u}_2 &= RHS_2 - T_C \cdot {}^N DCM^C[2,3] \\ m_H \dot{u}_3 &= RHS_3 - T_C \cdot {}^N DCM^C[3,3] \end{aligned} \tag{9}$$

whereas those for rotation are:

$$\begin{aligned} I_{H11} \dot{u}_4 &= RHS_4 + T_C d_{P^H - H^O,3} s_7 c_8 \\ I_{H22} \dot{u}_5 &= RHS_5 + T_C d_{P^H - H^O,3} s_8 \\ I_{H33} \dot{u}_6 &= RHS_6 \end{aligned} \tag{10}$$

where RHS_i is the right-hand side of the corresponding equations in (3) and (4) and ${}^N DCM^C = {}^N DCM^F \cdot {}^F DCM^C$ (see Table I).

C. Analysis of tether influence in system dynamics

When analyzing the equations (3) and (4) corresponding to helicopter dynamics in free flight, it is clear that rotational dynamics are not coupled with translational dynamics, which means the relationship between rotational and translational dynamics can be expressed as a unidirectional influence rotation $\Rightarrow$ translation. In contrast, in the dynamic equations of the tethered configuration given by (9) and (10) there is an additional force acting on the helicopter due to tether tension which produces in turn a moment affecting rotational dynamics, since the application point of the force does not exactly correspond with the helicopter's center of mass. This moment depends on both the helicopter's translational motion and orientation. Thus, the relationship between rotational and translational dynamics is now more complex, given a bidirectional influence rotation $\Leftrightarrow$ translation.

Following the analysis of (9) and (10), it can be concluded that the tether effect on the system is twofold. On the one hand, upon examination of translational dynamics, it is clear that the tether tension provides robustness against external disturbances such as lateral and longitudinal wind forces, since the projection of this force on the horizontal plane is always opposite to the direction of the resultant disturbance force. On the other hand, the moment induced by the existing offset between the tether tension application point P^H and center of mass H^O, produces undesired coupling between rotational and translational dynamics, which makes it more difficult to control the system. It is important to note that the value of the moment caused by the tether could be similar to or greater than the moments required to control the rotation of the helicopter in free flight without a tethering device.

Therefore, although it is true that high values of tether tension would reinforce stabilizing action in translational dynamics, it should also be taken into account that the higher this value is, the higher the control degradation for helicopter rotational dynamics may be. A trade-off criterion suggests that the maximum value of tether tension for system operation should be defined in such a way that the induced tether moment is always less than the maximum moment exerted by the main rotor control action, corresponding to cyclic pitch saturation.

III. Helicopter Control

The control structure adopted for the tethered system is based on the control scheme for the free helicopter presented in [9] (see Fig. 3). The gray blocks denote helicopter dynamics, whilst the white blocks denote the controller itself.

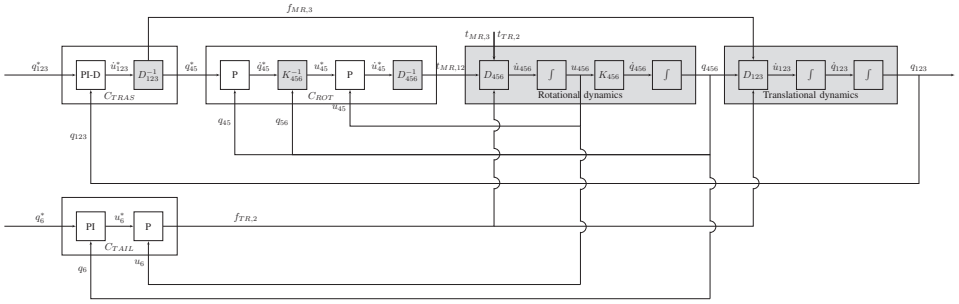

Fig. 3: General scheme for helicopter control

The underlying approach is based on linearization through model inversions and PID control laws. The main idea is to adjust the orientation of the main rotor plane, and therefore of the lifting force, in order to generate the translational accelerations required to reduce position error. The inputs for the control scheme are given by the desired position $q^*_{1,2,3}$ and the desired yaw angle q^*_6.

As can be seen in Fig. 3, the complete scheme consists of three control loops. The outer loop controller C_{TRAS} calculates from error between measured and desired position the required translational accelerations $\dot{u}^*_{1,2,3}$ to reduce such deviations, and this is implemented by means of a PI-D control law. These accelerations are converted into the desired orientation for the main rotor plane $q^*_{4,5}$, and the desired lifting force $f_{MR,3}$, through the inversion of translational dynamics in block D^{-1}_{123}. For the purpose of this inversion, input $f_{TR,2}$ is considered a disturbance and hence ignored ($f_{MR,3}$ is about one order of magnitude greater than $f_{TR,2}$). Resulting expressions after algebraic manipulation of (3) are given by:

$$\begin{aligned} f_{MR,3} &= m_H \sqrt{\left(\dot{u}^*_1\right)^2 + \left(\dot{u}^*_2\right)^2 + \left(\dot{u}^*_3 + g\right)^2} \\ q^*_5 &= \arcsin\left(\frac{m_H \dot{u}^*_1}{f_{MR,3}}\right) \\ q^*_4 &= \arcsin\left(-\frac{m_H \dot{u}^*_2}{f_{MR,3}\cos\left(q^*_5\right)}\right) \end{aligned} \tag{11}$$

The desired orientation for the main rotor plane $q^*_{4,5}$ given by C_{TRAS} is controlled in the inner loop C_{ROT} through calculation of moments $t_{MR,1}$ and $t_{MR,2}$. To this end, the desired Euler angle derivatives $\dot{q}^*_{4,5}$ are calculated from error between estimated Euler angles through Inertial Measurement Unit (IMU) data and the desired values $\dot{q}^*_{4,5}$ using a Proportional Gain. These Euler angle derivatives are then converted into the desired angular speeds $u^*_{4,5}$ in block K^{-1}_{456} by means of the inversion of rotational kinematics given by (2). Then, desired angular accelerations $\dot{u}^*_{4,5}$ are calculated from deviations between measured angular speed and the desired values $u^*_{4,5}$ using another Proportional Gain. The resulting angular accelerations are converted into moments $t_{MR,1}$ and $t_{MR,2}$ by the corresponding inversion of rotational dynamics in block D^{-1}_{456}. Again considering $f_{TR,2}$ and $t_{TR,2}$ as disturbances, and assuming $u_6 = 0$ (tail rotor controlled dynamics are several times faster than angular dynamics in longitudinal and lateral axes), algebraic manipulation of (4) yields:

$$\begin{aligned} t_{MR,1} &= K_{4p4}\dot{u}^*_4 - K_{45}\int \dot{u}^*_5 dt \\ t_{MR,2} &= K_{5p5}\dot{u}_5 - K_{54}\int \dot{u}^*_4 dt \end{aligned} \tag{12}$$

Finally, the desired yaw angle q^*_6 is controlled separately with the third loop controller C_{TAIL}. For this purpose, desired angular speed u^*_6 is calculated from error between estimated yaw angle through IMU measurements and the desired value q^*_6 using a PI control law. Tail rotor force $f_{TR,2}$ is then calculated from error between measured angular speed and the desired value u^*_6 using a Proportional Gain.

In order to tune the controller parameters, a classic pole assignment method is used for the system resulting from the linearization though model inversion. An analysis of the mechanical limitations of the system by means of experiments providing step inputs suggests that the closed-loop poles should be set around -1 for translational and rotational dynamics, and one order of magnitude greater for tail rotor dynamics. This is a trade-off value that guarantees a proper dynamic range, while the mechanical limitations of the system are not overreached.

A. Controller extension for tether-guided landing

In order use the tether as a guiding element while taking advantage of its stabilizing properties, a proper control design is needed. To this end, two modifications of the basic structure of Fig. 3 are proposed. Firstly, the maximum desired lifting force $f_{MR,3}$ at controller output is limited. This saturation value is set to approximately 120% of lifting force at free hover ($\overline{f_{MR,3}} \approx 1.2\, f_{MR,3}|^{hov}$). This means that if the system operates at about a nominal tether tension of $T^*_C \approx 0.2\, f_{MR,3}|^{hov}$, lifting force will be saturated and small tension variations will turn instantaneously into vertical motion, which allows landing by simply pulling the tether. Secondly, the PI-D block is changed to a P-D after hovering equilibrium when nominal tension of $T^*_C \approx 0.2\, f_{MR,3}|^{hov}$ is reached. The values from the integral terms are captured at this moment and provided to the controller during the entire landing maneuver. With the integral terms switched off, motion produced by small tension variations and other disturbances will not cause the desired lifting force signal to

vary too much from the saturation point, as nonzero position errors will no longer be integrated.

B. Controller extension for counteracting tether tension-induced moment

In order to account for undesired rotational influence of the tether tension-induced moment, a feed-forward action is proposed based on a tether tension vector estimation. To this end, a force sensor (load cell) is used to measure tension magnitude. Additionally, in order to establish the orientation of the tension vector, the universal joint holding the tether includes two magnetic encoders for measuring the angles. Once the measurements of tension magnitude T_C^m and universal joint angles $q_{7,8}^m$ are available, the tether moment is calculated as follows

$$\begin{aligned} \mathbf{M}_C &= \mathbf{p}^{P^H \to H^O} \times \mathbf{T}_C \\ M_{C,1} &= \mathbf{M}_C \cdot \mathbf{f_1} = T_C^m d_{P^H - H^O,3} \sin\left(q_7^m\right) \cos\left(q_8^m\right) \\ M_{C,2} &= \mathbf{M}_C \cdot \mathbf{f_2} = T_C^m d_{P^H - H^O,3} \sin\left(q_8^m\right) \end{aligned} \tag{13}$$

and then subtracted from the control moments $t_{MR,1,2}$ calculated for the free helicopter according to Fig. 3.

C. Tether-based position estimate for GPS replacement

In addition to the advantages in terms of stabilizing properties, the use of the tether provides an alternate position estimate for the controller, while its reliability will not be affected by the lack of GPS accuracy. To this end, the magnetic encoders measurement of the tether attitude relative to the helicopter is used. Additionally, a radar altimeter is incorporated into the system to acquire altitude information.

Assuming that tether tension is maintained about nominal value T_C^* during landing mode (tether lies on a straight line), the position estimate relative to tether's fixed point at ground N^O is made in two steps. Firstly, assuming the helicopter altimeter is near point P^H, and taking into account ${}^N DCM^C$ (see Table I), tether length q_9 is estimated using the altitude measurement given by q_3^{alt}, as depicted in Fig. 1, i.e.

$$\begin{aligned} q_3^{alt} &= q_9 \mathbf{c_3} \cdot \mathbf{n_3} \Rightarrow \\ \hat{q}_9 &\approx q_3^{alt} / \left({}^N DCM^C\left[3,3\right]\right) \end{aligned} \tag{14}$$

Once this calculation is made, a straightforward estimate of helicopter linear position relative to the tether's fixed point ground can be made by using (7) and assuming $q_9 \gg d_{P^H - H^O,3}$:

$$\begin{aligned} \sum_{i=1}^{3} \left(q_i \mathbf{n}_i\right) &\approx \hat{q}_9 \mathbf{c_3} \Rightarrow \\ \hat{q}_1 &\approx \hat{q}_9 \mathbf{c_3} \cdot \mathbf{n_1} = \hat{q}_9 {}^N DCM^C\left[1,3\right] \\ \hat{q}_2 &\approx \hat{q}_9 \mathbf{c_3} \cdot \mathbf{n_2} = \hat{q}_9 {}^N DCM^C\left[2,3\right] \end{aligned} \tag{15}$$

Note that ${}^N DCM^C = {}^N DCM^C\left(\hat{q}_4, \hat{q}_5, \hat{q}_6, q_7^m, q_8^m\right)$ is a function of estimated Euler angles $\hat{q}_{4,5,6}$ through IMU measurements and measured universal joint angles $q_{7,8}^m$ only.

The velocity estimate $\hat{u}_{1,2}$ is directly calculated by backward numerical differentiation of the position estimate $\hat{q}_{1,2}$.

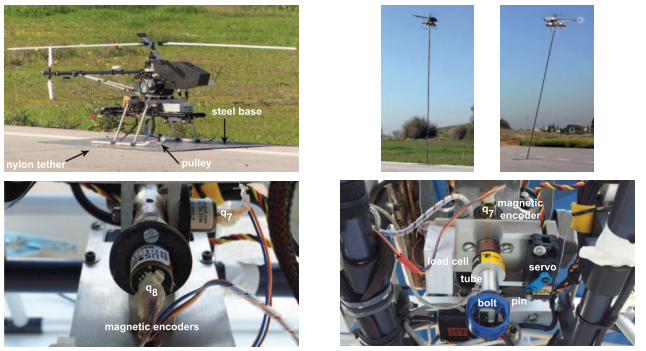

(a) Top: Aero-Tech CB-5000 helicopter. Bottom: magnetic encoders

(b) Top: experiments in progress. Bottom: load cell and safety release mechanism

Fig. 4: Experimental setup

In order to handle encoder noise due to joint vibrations, the position estimate is filtered using a discrete Butterworth filter.

IV. Experimental results

A. Experimental setup

The experiments were performed with an unmanned helicopter based on the Aero-Tech CB-5000 platform shown in Fig. 4a. This helicopter has a rotor diameter of $1.8\,m$ and a main rotor speed of approximately $1300\,rpm$, powered by a $1.8\,kW$ two-stroke engine. The helicopter was equipped with an IMU for measuring angular speed and estimating Euler angles, a high precision radar altimeter for measuring altitude, and a RTK system which allows comparison of the tether-based estimates with a reliable reference. The helicopter was tethered with a nylon rope. For that purpose, a heavy steel plate with an area of approximately $1\,m^2$ was placed on the ground just below the helicopter. A pulley was soldered to this base in order to allow application of tension to the tether from a safe distance. As previously mentioned, the tether was connected to the helicopter using a a two-axis universal joint with one magnetic encoder attached to each axis as shown in the Fig. 4a. Below the joint, a load cell to measure the tether tension and a safety release mechanism were placed as seen in Fig. 4b. This mechanism consisted of a bolt inserted into a tube and fixed inside by a pin which can be pulled out by a servo to release the tether. The servo can be triggered remotely by the safety pilot.

B. Experiment 1: Tether tension stabilizing action at hover

The goal of this experiment was to verify the stabilizing action of tether tension in translational dynamics predicted upon analysis of the mechanical model. To that end, disturbances consisting of two consecutive steps in the lateral position reference q_2^* were applied at hover (see Fig. 5). The two time intervals of the figure correspond to operation with and without applied tension. It is clear that the effect of disturbance on lateral position q_2, as well as the amplitude of longitudinal position q_1 oscillations, are reduced when tension is applied to the tether, as can be observed by the standard deviations (σ).

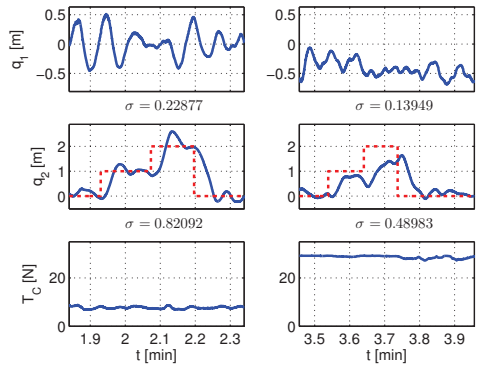

Fig. 5: Experiment 1. Left: without applied tension. Right: with applied tension. Top: RTK longitudinal position q_1. Middle: RTK lateral position q_2 (Solid) and reference q_2^* (Dotted). Bottom: load cell tension measurement

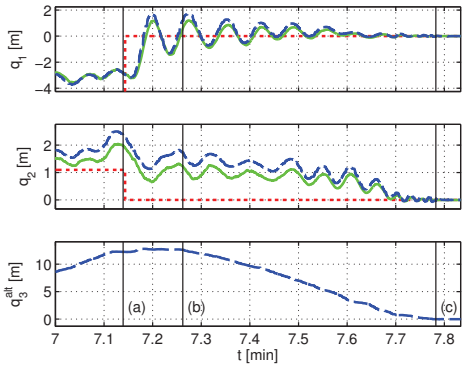

Fig. 6: Experiment 2. Top: tether-based estimate $\hat{q}_1$ (Solid), RTK measured q_1 (Dashed) and desired q_1^* (Dotted) longitudinal position. Middle: tether-based estimate $\hat{q}_2$ (Solid), RTK measured q_2 (Dashed) and desired q_2^* (Dotted) lateral position. Bottom: altimeter measurement q_3^{alt} (Dashed)

C. Experiment 2: Tether-guided landing without GPS

In this experiment the objective was the validation of the tether-guided landing approach without using the GPS sensor. The results are shown in Fig. 6 and supplementary video attachment[1]. During the entire landing maneuver, the controller operation was based on the tether-based estimation of linear position. Furthermore, in order to analyse the accuracy of position estimate, the graphs also include the position measured by the RTK system. Absolute values of maximum error are less than $0.9\,m$ and $0.6\,m$ for q_1 and q_2 respectively. It can also be observed that error decreases as altitude decreases.

After hovering with nominal tension applied to the tether, the landing maneuver consisted of three phases. As can be seen, at the time marked (a), the reference for relative longitudinal and lateral position was set to zero, which means the controller tried to maintain the helicopter on the vertical line over the tether's fixed point at ground. At the time marked (b) the tether was pulled down gently, thus altitude started to decrease slowly. Finally, at time marked (c) the helicopter touched down. As can be observed, the landing was successful with 100% accuracy with respect to the tether's fixed point at ground.

V. Conclusion

This paper extends the authors' previous contributions regarding the use of tethered configurations for improving performance of unmanned helicopters. More precisely, this work addresses two important issues when dealing with hovering and landing maneuvers: the effects of disturbances and sensor reliability.

Regarding sensor reliability, the often problematic GPS measurement has been replaced by an alternative linear position estimate based on measuring helicopter altitude and tether attitude relative to the airframe. The validity of this new sensing approach has been demonstrated in successful landing experiments. Although the estimate accuracy is sufficient to allow a safe landing maneuver, the design of a suitable observer to improve results seems to be a logical continuation of this work. Concerning hovering performance, the results have also endorsed the analysis which showed stabilizing properties of the tethered configuration in translational dynamics.

Since position estimate is relative to the landing point, it is also worth mentioning that the sensing and control approach proposed in this paper can potentially be used for tether-guided landing on moving platforms. New experiments will be performed in future in order to explore this possibility.

[1]A higher resolution video can also be seen at http://grvc.us.es/staff/sandino/videos/ICRA2014

Acknowledgments

The authors want to thank the Center for Advanced Aerospace Technologies (CATEC) for providing all the necessary means to perform the experiments. Very special thanks also to Allan Bell for his invaluable help as safety pilot.

References

[1] B. Ahmed and H. Pota, "Backstepping-based landing control of a RUAV using tether incorporating flapping correction dynamics." Proceedings of the American Control Conference, 2008, pp. 2728–2733.

[2] S. Oh, K. Pathak, S. K. Agrawal, H. R. Pota, and M. Garratt, "Approaches for a tether-guided landing of an autonomous helicopter," *IEEE Transactions on Robotics*, vol. 22, no. 3, pp. 536–544, 2006.

[3] L. Sandino, M. Bejar, K. Kondak, and A. Ollero, "On the use of tethered configurations for augmenting hovering stability in small-size autonomous helicopters," *Journal of Intelligent & Robotic Systems*, vol. 70, pp. 509–525, 2013.

[4] ——, "Improving hovering performance of tethered unmanned helicopters with nonlinear control strategies." Proceedings of the International Conference on Unmanned Aircraft Systems, 2013, pp. 443–452.

[5] D. Rye, "Longitudinal stability of a hovering, tethered rotorcraft." *Journal of Guidance, Control, and Dynamics*, vol. 8, no. 6, pp. 743–752, 1985.

[6] G. Schmidt and R. Swik, "Automatic hover control of an unmanned tethered rotorplatform," *Automatica*, vol. 10, no. 4, pp. 393–403, 1974.

[7] T. R. Kane and D. A. Levinson, *Dynamics. Theory and Applications*. McGraw-Hill, 1985.

[8] L. Sandino, M. Bejar, and A. Ollero, "A survey on methods for elaborated modeling of the mechanics of a small-size helicopter. analysis and comparison," *Journal of Intelligent & Robotic Systems*, 2013.

[9] K. Kondak, M. Bernard, N. Losse, and G. Hommel, "Elaborated modeling and control for autonomous small size helicopters," *VDI Berichte*, vol. 1956, pp. 207–216, 2006.